

# Feasibility Study of a Search for R-Parity violating resonant Selectron Production at the LHC

Nils Hempelmann

Bachelorarbeit in Physik

vorgelegt der Fakultät für Mathematik, Informatik und Naturwissenschaften der  
RWTH Aachen im August 2012

angefertigt im

III. Physikalischen Institut A

bei

Prof. Dr. Thomas Hebbeker

## **Selbstständigkeitserklärung**

Ich versichere, dass ich die Arbeit selbstständig verfasst und keine anderen als die angegebenen Quellen und Hilfsmittel benutzt sowie Zitate kenntlich gemacht habe.

Aachen, den

## Abstract

In R-parity violating supersymmetric theories, resonant slepton production is possible. While resonant smuon production has been studied before at the Tevatron collider, it has been assumed that resonant selectron production is unobservable at the LHC because of limits coming from the search for neutrinoless double beta decay. The aim of this study is to determine whether these limits can be improved by a search for resonant selectron production at CMS. First results for 2011 data are presented.

It is shown that the search for resonant selectron production at CMS is feasible and that the limits from experiments using neutrinoless double beta decay can be significantly improved.

## Kurzdarstellung

In R-paritätsverletzenden supersymmetrischen Theorien ist resonante Sleptonenproduktion möglich. Resonante Smyonenproduktion wurde bereits am Tevatron untersucht, es wurde jedoch angenommen, dass resonante Selekttronenproduktion am LHC aufgrund von Grenzen aus der Suche nach neutrinolosem Doppelbetazerfall nicht beobachtbar ist. Ziel dieser Arbeit ist es festzustellen, ob diese Grenzen mit einer Suche nach resonanter Selekttronenproduktion bei CMS verbessert werden können. Es werden erste Ergebnisse für die Daten von 2012 vorgestellt.

Es wird gezeigt, dass die Suche nach resonanter Selekttronenproduktion bei CMS machbar ist und dass die Grenzen aus Experimenten mit neutrinolosem Doppelbetazerfall signifikant verbessert werden können.

# Contents

<b>1</b>	<b>Theoretical Background</b>	<b>5</b>
1.1	The Standard Model of Particle Physics . . . . .	5
1.2	Supersymmetry . . . . .	5
1.3	Sparticle Production and Possible Decay Modes at the LHC . . . . .	7
<b>2</b>	<b>LHC and CMS</b>	<b>8</b>
<b>3</b>	<b>Existing Limits for <math>\lambda'_{111}</math></b>	<b>11</b>
3.1	Neutrinoless Double Beta Decay . . . . .	11
3.2	Boundaries from Neutrino Masses . . . . .	13
<b>4</b>	<b>Analysis</b>	<b>14</b>
4.1	Object Identification . . . . .	14
4.2	Event Selection . . . . .	17
4.3	Pileup Reweighting . . . . .	19
4.4	Tight to Loose Ratio . . . . .	19
4.5	Jet Smearing . . . . .	21
4.6	Results . . . . .	23
4.7	Calculation of Limits . . . . .	25
<b>5</b>	<b>Conclusion</b>	<b>27</b>

# 1 Theoretical Background

## 1.1 The Standard Model of Particle Physics

The Standard Model of particle physics [2, 3, 4] is a relativistic quantum field theory describing the composition of matter and three of the four known fundamental interactions: the strong, the weak and electromagnetic interaction. Gravity is currently best described by the general theory of relativity. Finding a quantum theory of gravity is an active area of research.

In the Standard Model, matter consists of quarks and leptons. The quarks and leptons can be divided into three generations, which are roughly ordered by mass in increasing order. Each generation contains two quarks and two leptons, one of the leptons is a neutrino. The quarks have an electric charge of  $+2/3$  or  $-1/3$ , for antiquarks the signs are reversed. Neutrinos are electrically neutral, the remaining leptons have a charge of  $\pm 1$ .

All fundamental interactions in the Standard Model are mediated by gauge bosons. The electromagnetic interaction is mediated by photons. It affects all particles with an electric charge.

The weak interaction is mediated by two different kinds of gauge bosons, the  $W^\pm$  boson and the  $Z^0$  boson. Unlike the other gauge bosons, the  $W^\pm$  and  $Z^0$  have a mass of 80.4 and 91.2  $GeV$ , respectively. This mass limits the range of the weak interaction, the typical range is around  $10^{-17}$  to  $10^{-16} m$ . The weak interaction is the only interaction that can change the flavor of a quark and the only interaction that violates parity. It affects all leptons and quarks.

The strong interaction is mediated by gluons. It only affects quarks and gluons. The strong interaction is related to the so-called color charge, which can have the values red, green, blue, antired, antigreen and antiblue. Gluons have one color and one anticolor, quarks have one color and antiquarks have one anticolor. As gluons have a color charge, they can couple to each other. Isolated quarks do not exist, all particles that can be directly observed are color neutral. In analogy to the additive mixing of colors, a color neutral particle can be constructed by combining red, blue and green or their respective anticolors (Baryons) or one color and one anticolor (Mesons).

The Standard Model also postulates the so-called Higgs boson. A boson with a mass of 125  $GeV$  has recently been discovered at the LHC [5]. This particle could be the Higgs boson.

## 1.2 Supersymmetry

The Standard Model has been very successful and is well validated by experimental evidence. However there are several attempts to expand the Standard Model as it cannot explain phenomena like dark matter, which was predicted due to astronomical observations, or the hierarchy problem. One approach to this is supersymmetry.

In supersymmetric theories [1], each particle is associated with a superpartner or sparticle. The superpartner of a fermion is a boson and vice versa. If supersymmetry was an unbroken symmetry, two superpartners should have the same mass and quantum numbers, except for the spin. However, no sparticles have been detected yet. This means that

sparticles have a much higher mass than their superpartners and that supersymmetry, if it exists, is a broken symmetry.

The supersymmetric extension of the Standard Model with the smallest number of additional particles is the Minimal Supersymmetric Standard model (MSSM), adding one additional Higgs doublet and a superpartner for each particle in the Standard Model. Sparticles are denoted using a tilde. For bosonic sparticles, an “s” is added at the beginning of the name of the Standard Model particle, in case of fermions the suffix “-ino” is added. Thus, the superpartner of the electron,  $e$  is the selectron,  $\tilde{e}$ , the superpartners of the gauge bosons are the neutralinos and the charginos.

In the most general supersymmetric Standard Model the proton has a short lifetime, which is not in agreement with the experimental limits. To prevent this, an additional symmetry must be imposed on the model [8].

One possibility, which is used in the MSSM, is to introduce a new conserved quantum number called R-parity. R-parity is defined as  $P_R = (-1)^{2s+3B+L}$ , where  $s$  is the spin,  $B$  is the baryon number and  $L$  is the lepton number. The particles of the Standard Model have an R-parity of 1, while the sparticles have an R-parity of -1. If R-parity is conserved, the lightest sparticle (LSP) must be stable, making it a potential candidate for dark matter. Another implication is that sparticles can only be produced in pairs, making resonant particle production impossible in this model.

The large number of parameters in MSSM can be reduced by making additional assumptions at the GUT-scale, leading to the minimal supergravity model (mSUGRA). This model has five parameters in addition to those of the Standard Model:

- $M_0$ , the universal scalar mass
- $M_{1/2}$ , the gaugino mass
- $A_0$ , the trilinear scalar coupling
- $\tan\beta$ , the ratio of the Higgs vacuum expectation values
- $\text{sgn}\mu$ , the sign of the bi-linear Higgs mixing parameter

The masses of the various sparticles can be calculated from these parameters.

This paper deals with the R-parity-violating mSUGRA model [7]. Instead of R-parity, baryon triality is imposed to assure the stability of the proton [6]. Baryon triality only allows baryon number violation if the difference is an integer multiple of three [7]. In this model there are additional parameters  $\lambda_{ikj}$ ,  $\lambda'_{ikj}$  and  $\lambda''_{ikj}$  describing the R-parity-violating couplings. The indices represent the particle families involved in the vertex. Terms proportional to  $\lambda_{ikj}$  or  $\lambda'_{ikj}$  violate lepton number, term proportional to  $\lambda''_{ikj}$  violate baryon number.

### 1.3 Sparticle Production and Possible Decay Modes at the LHC

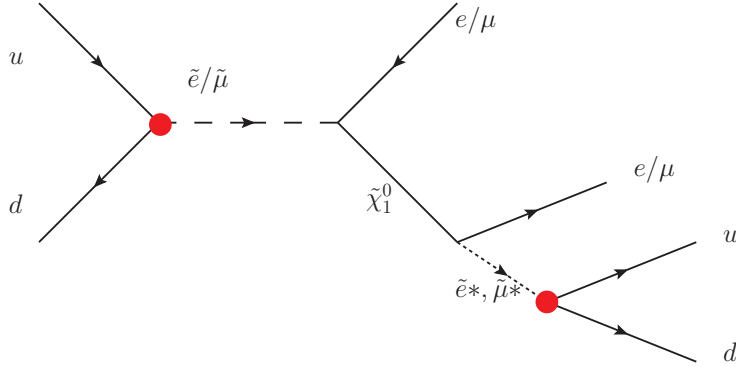


Figure 1: Typical resonant slepton production and decay. The R-parity-violating vertices are highlighted in red.

A typical process for resonant slepton production and decay can be seen in Fig. 1. The production of selectrons and smuons happens in analogous processes. In the former case, the leptons are electrons, in the latter case muons.

The slepton is formed in an R-parity violating process from two quarks. It decays into a neutralino and a lepton. The neutralino decays forming two jets and another lepton. As the neutralino is a Majorana particle, the two leptons can have the same or different signs. This analysis uses events with same-sign electrons as the Standard Model background is smaller than for opposite-sign electrons. Most Standard Model processes only produce electron-positron pairs.

The process involves two R-parity-violating vertices, the matrix elements are thus proportional to  $\lambda'_{111}$  for selectron production or  $\lambda'_{211}$  for muon production. Whether this process can actually be observed at the LHC depends on the values of the coupling constants [13].

While resonant smuon production has been searched for before at the Tevatron [19], it was assumed that the existing limits on  $\lambda'_{111}$  could not be improved at a collider. The LHC has a significantly higher center of mass energy. The aim of this study is to determine whether the limits from the LHC can be stricter than the existing ones.

## 2 LHC and CMS

The Large Hadron Collider (LHC) is a particle accelerator and collider located close to Geneva (Switzerland) that started producing collisions in 2009. Depending on the operation mode it can collide beams of protons or lead nuclei. In case of protons, it is designed to achieve a center-of-mass energy of  $14\text{TeV}$ ; as of 2012 it has reached  $8\text{GeV}$ . The LHC is a circular collider with a circumference of almost  $27\text{km}$ . The design luminosity of the LHC is  $10\text{nb}^{-1}\text{s}^{-1}$ , currently it is  $6\text{nb}^{-1}\text{s}^{-1}$  [21]. There are four large detectors at the LHC: ATLAS, CMS, ALICE and LHCb. This thesis uses data from the CMS experiment.

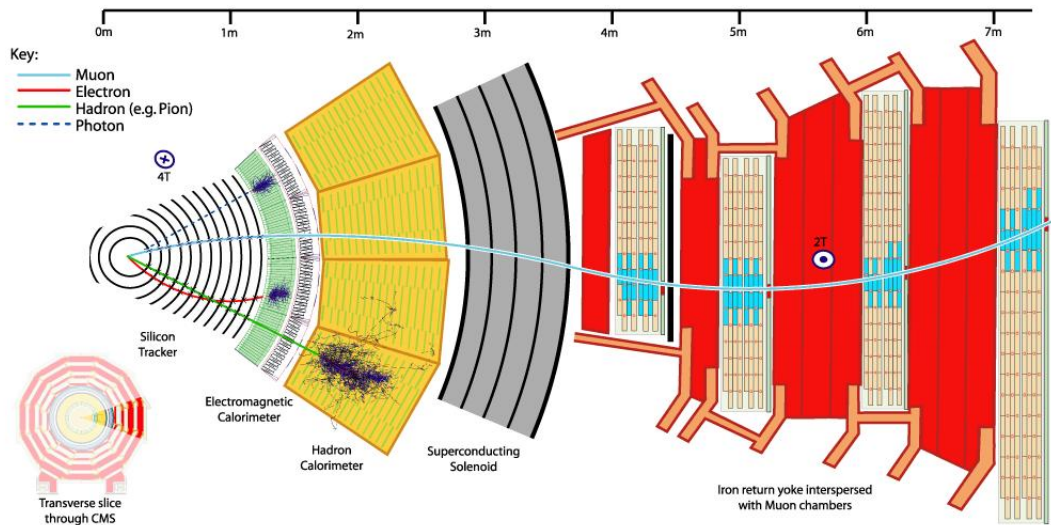


Figure 2: Cross section of the CMS-detector with tracks from different particles [22].

CMS stand for Compact Muon Solenoid. It is a cylindrical detector with a diameter of  $15\text{m}$  and a length of  $21\text{m}$ . CMS consists of a barrel section and two endcaps made of different components. Figure 2 shows a cross section of the barrel.

- The innermost part of CMS is a silicon tracker which consist of several concentric layers and the two endcaps. The first three layers are pixel detectors with a pixel size of  $100 \cdot 150\ \mu\text{m}^2$  followed by ten layers of microstrip detectors with a strip pitch varying between  $80\ \mu\text{m}$  and  $120\ \mu\text{m}$ . The tracking volume has a length of  $5.6\text{m}$  and a diameter of  $2.2\text{m}$ . The data from the tracker is used to match the particles to the vertices at which they originated. The curvature of the tracks is used to determine the particles' momentum and charge.
- The next detector is the electromagnetic calorimeter (ECAL) measuring the energy of electrons and photons. It is made of 61200 lead tungstate crystals in the barrel section and 7324 in each endcap. The light induced by particle showers is measured

using photodiodes. Most electrons and photons are absorbed in the calorimeter, while other particles lose only some energy.

- The hadronic calorimeter (HCAL), together with ECAL, measures the energy of hadrons. It consists of several absorber layers made of brass and steel and interleaved scintillator layers. As the hadrons pass the absorber layers, they emit photons and electrons that can be detected in the scintillator layers. As hadrons originate from the hadronization of individual quarks and gluons they appear in narrow cones called jets that are reconstructed using ECAL, HCAL and tracker measurements.
- The magnetic field for CMS is generated by a superconducting solenoid coil located between the HCAL and the muon chambers. The magnetic field is amplified by iron yokes between the muon chambers. The flux density is  $4T$  inside and about  $2T$  at the muon chambers. The strong field is necessary to measure the charge and the momentum of the particles accurately.
- The outermost detector part is the muon chambers, which use different types of gas detectors. Muons are the only particles that are able to pass through the other detector parts and reach the muon chambers.

Electrons create a signal in the tracker and in the ECAL. Photons only leave a signal in the ECAL. Hadrons leave a signal in the tracker and the HCAL, they also create a smaller signal in the ECAL. Muons leave signals in the tracker and the muon chambers, and little energy in the ECAL and HCAL.

At design luminosity, there will be around  $10^9$  interactions per second, but only about 400 can be recorded. Therefore, the events have to be filtered to select only those that are interesting for analyses. The data selection is a two-step procedure. The Level-1 trigger performs a first selection based on the data of the muon chambers and the calorimeters. It checks for the presence of objects like HCAL and ECAL energy deposits and muons, but does not perform a complete reconstruction of all objects. The Level-1 trigger is hardware-based and has an output rate of about  $75\text{ kHz}$ .

The second step is the software-based High-Level Trigger (HLT). It further reduces the number of events and roughly categorizes them depending on the objects appearing in the event [20, 22].

CMS uses the following coordinate convention:

- The z-axis runs counterclockwise along the beam direction, the x-axis points towards the center of the LHC, the y-axis points upwards.
- The azimuth angle  $\phi$  is defined by the relation  $\tan \phi = \frac{x}{y}$ .
- The polar angle  $\theta$  is parametrized using the pseudorapidity  $\eta = -\ln\left(\tan\left(\frac{\theta}{2}\right)\right)$ . For high energies where  $E \approx |p|$  the pseudorapidity has about the same value as the rapidity  $y = \frac{1}{2} \ln\left(\frac{E+p_L}{E-p_L}\right)$ , where  $p_L$  is the longitudinal momentum and  $E$  is the energy. This approximation has the advantage that it does not depend on the

particle's mass. Differences in  $y$  and hence differential cross sections in the form  $\frac{d\sigma}{dy}$  are invariant under Lorentz boosts along the z-axis.

- The “distance” between two objects in  $\eta, \phi$ -space is defined as  $\Delta R = \sqrt{\Delta\eta^2 + \Delta\phi^2}$ .

### 3 Existing Limits for $\lambda'_{111}$

The existing limits from  $\lambda'_{111}$  are stricter than those for  $\lambda'_{211}$ . A search for resonant selectron production at a collider like LHC only makes sense if the discovery reach is greater than the existing limit. The most stringent limit comes from neutrinoless double beta decay (section 3.1), a process that is predicted by R-parity violating theories but that has not been observed in experiments.

As the mSUGRA model predicts non-zero neutrino masses that depend on the  $\lambda_{ijk}$  and  $\lambda'_{ijk}$  coupling constants, cosmological limits on the neutrino masses also provide limits on these constants (section 3.2).

#### 3.1 Neutrinoless Double Beta Decay

Double beta decay is the simultaneous decay of two neutrons in one atomic nucleus into protons while emitting two electrons and two electron neutrinos. The decay rate of this process is much slower than that of normal beta decay, so it can only be experimentally observed in isotopes where normal beta decay is energetically impossible. Double beta decay has been observed in twelve different isotopes [15].

Neutrinoless double beta decay ( $0\nu\beta\beta$ ) is a similar process without an emission of neutrinos which has not been experimentally observed. As this process violates lepton number conservation it is not possible in the Standard Model. However, several theories beyond the Standard Model predict neutrinoless double beta decay. Neutrinoless double beta decay has been studied in various experiments such as the Heidelberg-Moscow experiment [16] or NEMO [17]. Within the RPV mSUGRA model, there are several mechanisms that contribute to  $0\nu\beta\beta$ . Neutrinos can be Majorana fermions, meaning that they are their own antiparticles.  $0\nu\beta\beta$  is then possible by exchanging a neutrino in a process similar to normal beta decay (Fig. 3).

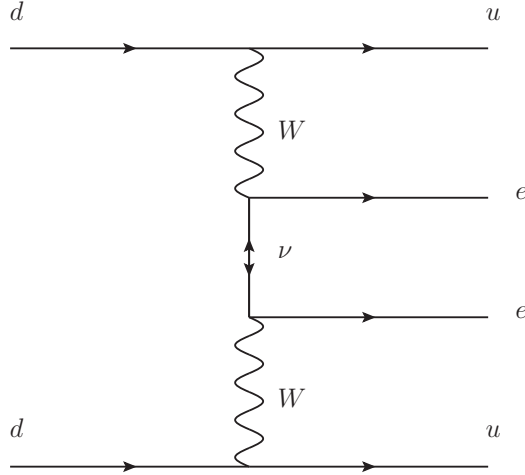


Figure 3: Neutrinoless double beta decay via exchange of a Majorana neutrino. [13]

There is also a “direct” contribution from the couplings  $\lambda'_{113}\lambda'_{131}$  and  $\lambda'_{111}\lambda'_{111}$ , for example the process in Fig. 4.

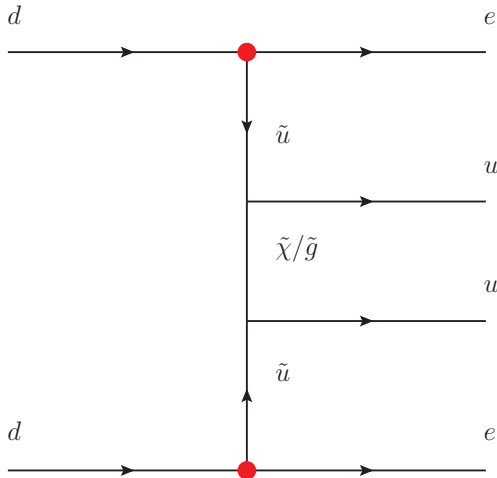


Figure 4: Example for a  $\lambda'_{111}$  contribution to neutrinoless double beta decay. The RPV-violating vertices are highlighted in red.

Consequently, the limits on the half-life of neutrinoless double beta decay lead to limits on the Majorana mass of the electron neutrino and the R-parity violating couplings, in particular  $\lambda'_{111}$ . In the most general case, Majorana neutrinos,  $\lambda'_{111}$  and  $\lambda'_{113}\lambda'_{131}$  all contribute to  $0\nu\beta\beta$ . The effects may interfere constructively or destructively. Assuming that the contribution from Majorana neutrinos is negligible, the limit on  $\lambda'_{111}$  from this calculation is [18]

$$\lambda'_{111} < 3.3 \cdot 10^{-4} \cdot \left( \frac{m_{\tilde{q}}}{100 \text{ GeV}} \right)^2 \cdot \left( \frac{m_{\tilde{g}/\tilde{\chi}}}{100 \text{ GeV}} \right)^{1/2} \quad (1)$$

This limit was calculated using the limit on the neutrinoless double beta decay of the germanium isotope  $^{76}\text{Ge}$ ,  $T_{1/2} > 1.1 \cdot 10^{25} \text{ yrs}$ . The limit scales with  $\sqrt[4]{T_{1/2}}$ , so increases in the limit on the half-life only result in small improvements in the limit on  $\lambda'_{111}$  [18]. Using the newer value of  $1.9 \cdot 10^{25} \text{ yrs}$  [16] decreases the prefactor to about  $2.9 \cdot 10^{-4}$ .

This is currently the best limit on  $\lambda'_{111}$ . As indicated in the formula, the limit depends on the masses of the squark and the gluino and thus on the mSUGRA parameters. In the following, the mass spectrum is calculated using the program SOFTSUSY [10, 11, 33].

For low values for  $M_{1/2}$  and  $M_0$ , the sparticle masses are around  $100 \text{ GeV}$ , leading to a very low limit that makes selectron production unobservable [13]. As the sparticle masses increase with the mSUGRA parameters, the limit is looser for higher values.

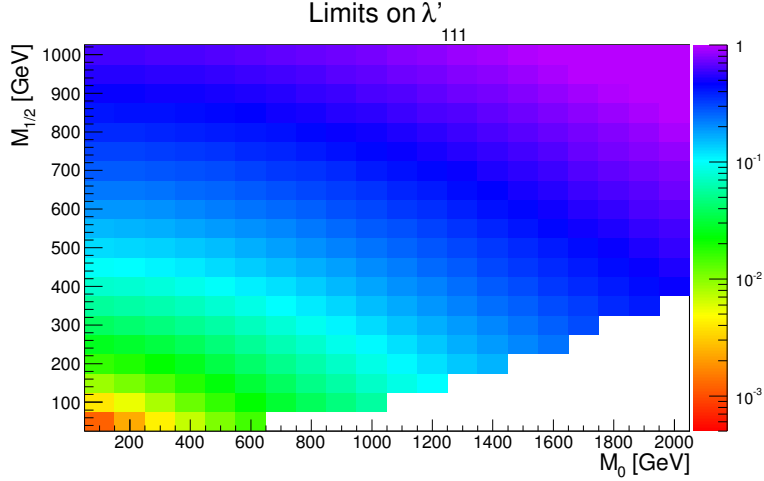


Figure 5: Limits on  $\lambda'_{111}$  from neutrinoless double beta decay according to equation (1). The particle masses were calculated using SOFTSUSY assuming  $A_0 = 0$ ,  $\tan \beta = 20$  and  $\text{sgn } \mu = 1$ . The limit varies from  $10^{-3}$  to 1, showing the strong dependence on the particle mass spectrum. The limit is very strict for low  $M_{1/2}$  and  $M_0$ .

### 3.2 Boundaries from Neutrino Masses

While neutrinos do not have a mass in the Standard Model, the observation of neutrino oscillation indicates that neutrinos have non-zero masses. The strictest limit on the neutrino masses comes from the anisotropy of the cosmic background radiation, which leads to the inequality  $\sum_{i=e,\mu,\tau} m_{\nu_i} < 0.41 \text{ eV}$ . The R-parity violating mSUGRA model also predicts neutrino masses, which must be in accordance with the experimental limit. As the predicted masses depend on the  $\lambda_{ijk}$  and  $\lambda'_{ijk}$  coupling constants, this limits their possible range of values (Table 1).

	Up Mixing			Down Mixing		
$A_0 [GeV]$	-100	500	550	-100	500	550
$\lambda'_{111} \cdot 10^{-3}$	2.0	27	83	0.97	13	53

Table 1: Limits on  $\lambda'_{111}$  from neutrino masses at the point SPS1a with  $M_0 = 100 \text{ GeV}$ ,  $M_{1/2} = 250 \text{ GeV}$ ,  $\tan \beta = 10$ ,  $\mu > 0$ . [9]

“Up mixing” and “down mixing” refer to different mixing of the quark states. There is also a strong dependence on  $A_0$ .

## 4 Analysis

The aim of this analysis is to estimate the search reach of a possible future search for resonant selectron production at CMS. The procedure used is based on an ongoing search for resonant smuon production [32] and has been adapted for electrons. The analysis determines the search sensitivity at ten different points in the  $M_0, M_{1/2}$  plane, which were chosen to match those in another thesis about resonant smuon production [12].

$M_0 [GeV]$	200	200	300	500	500	600	1000	1000	1600	1600
$M_{1/2} [GeV]$	100	250	500	100	250	850	200	500	450	850
$\lambda'_{111} \cdot 10^{-3}$	5.5	29.0	134.4	16.7	45.7	470.9	88.8	234.5	368.4	780.9

Table 2: Points in the  $M_0, M_{1/2}$  plane used in the analysis and limits from neutrinoless double beta decay. The other mSUGRA parameters are  $A = 0$ ,  $\tan\beta = 20$  and  $\text{sgn}\mu = 1$  for all points.

The analysis uses data recorded in 2011 with the CMS experiment, corresponding to an integrated luminosity of  $\mathcal{L} = 4.98 \pm 0.11 \text{ fb}^{-1}$ . The Monte Carlo datasets are listed in Table 3. The table includes Monte Carlo datasets for QCD and W+Jets processes, however they are only used for cross-checks. The background from these processes is estimated using the tight to loose ratio method. The signal Monte Carlo samples each have 50000 events. They are generated assuming  $\lambda'_{111} = 0.001$  at the GUT scale. In the plots they are scaled up to  $\lambda'_{111} = 0.01$ .

The data is processed on the grid using CMSSW 4.2.8 and ACSUSYANALYSIS [25]. As described in section 1.3, single selectron production produces two like-signed electrons, two jets and no missing transverse energy.

### 4.1 Object Identification

The object identification step defines the requirements for muons, electrons and jets to be used in the analysis. All vertices must have at least four degrees of freedom and be less than  $\Delta z = 24 \text{ cm}$  from the beamspot. The vertices must not be marked as fake.

Electrons are selected using a cut based ID [24]. The transverse momentum must exceed  $15 \text{ GeV}$ . There are various cuts assuring the electrons are well reconstructed. The exact values depend on whether the electron is found in the barrel ( $|\eta| < 1.4442$ ) or the endcap ( $1.566 < |\eta| < 2.5$ ), see Table 4. The variable  $\sigma_{i\eta i\eta}$  is the weighted root mean square of eta in a  $5 \cdot 5$  crystal area of a cluster in the ECAL. Electrons in the gap between the barrel and the endcap or with  $|\eta| > 2.5$  are ignored. All electrons must have a relative isolation of less than 0.15. The relative isolation is defined as the sum of the transverse momentum measured in the tracker and the transverse energy of other particles deposited in the ECAL and HCAL within a cone of  $\Delta R = 0.3$  around the electron divided by the electrons transverse momentum or by  $20 \text{ GeV}$  if the electrons

Process	Dataset Name	Cross Section [pb]	#Events
Drell- Yan	DYJetsToLL_M-10To50_TuneZ2_7TeV-madgraph	9611 (LO)	31277479
Drell- Yan	DYJetsToLL_TuneZ2_M-50_7TeV-madgraph-tauola	3048 (NNLO)	35982657
QCD	QCD_Pt-30to40_doubleEMEnriched_TuneZ2_7TeV-pythia6	10868 (LO)	6094669
QCD	QCD_Pt-40_doubleEMEnriched_TuneZ2_7TeV-pythia6	43571 (LO)	40281010
single top	Tbar_TuneZ2_s-channel_7TeV-powheg-tauola	1.44 (NNLL)	137647
single top	Tbar_TuneZ2_t-channel_7TeV-powheg-tauola	22.65 (NNLL)	1939460
single top	Tbar_TuneZ2_tW-channel-DR_7TeV-powheg-tauola	7.87 (NNLL)	322638
single top	T_TuneZ2_s-channel_7TeV-powheg-tauola	3.19 (NNLL)	259572
single top	T_TuneZ2_t-channel_7TeV-powheg-tauola	41.92 (NNLL)	3891502
single top	T_TuneZ2_tW-channel-DR_7TeV-powheg-tauola	7.87 (NNLL)	812544
$t\bar{t}$	TTJets_TuneZ2_7TeV-madgraph-tauola	165 (NNLL)	45759343
$W \rightarrow l\nu$	WJetsToLNu_TuneZ2_7TeV-madgraph-tauola	31314 (NNLO)	76184222
$WW \rightarrow 2l2\nu$	WWJetsTo2L2Nu_TuneZ2_7TeV-madgraph-tauola	4.78 (NLO)	1190173
$WZ \rightarrow 2l2q$	WZJetsTo2L2Q_TuneZ2_7TeV-madgraph-tauola	1.21 (NLO)	938462
$WZ \rightarrow 3l\nu$	WZJetsTo3LNu_TuneZ2_7TeV-madgraph-tauola	0.613 (NLO)	1196866
$ZZ \rightarrow 2l2\nu$	ZZJetsTo2L2Nu_TuneZ2_7TeV-madgraph-tauola	0.120 (NLO)	1078790
$ZZ \rightarrow 2l2q$	ZZJetsTo2L2Q_TuneZ2_7TeV-madgraph-tauola	0.416 (NLO)	908352
$ZZ \rightarrow 4l$	ZZJetsTo4L_TuneZ2_7TeV-madgraph-tauola	0.0602 (NLO)	1179976

Table 3: Monte Carlo datasets. The cross sections for the single top processes were calculated in [30], the cross sections for top pair production were calculated in [31]. The background from QCD and W+Jets processes are determined using the tight to loose ration method (section 4.4), the Monte Carlo data is used for cross-checks. The cross section of the QCD samples is corrected for filter efficiency.

transverse momentum is below  $20\text{ GeV}$ .

$$relIso = \left\{ \begin{array}{ll} \frac{p_{T,Trk} + E_{T,ECAL} + E_{T,HCAL}}{p_T}, & p_T > 20\text{ GeV} \\ \frac{p_{T,Trk} + E_{T,ECAL} + E_{T,HCAL}}{20\text{ GeV}}, & p_T < 20\text{ GeV} \end{array} \right\} \quad (2)$$

There are also individual cuts for  $p_{T,Trk}/p_T$ ,  $E_{T,ECAL}/E_T$ , and  $E_{T,HCAL}/E_T$ .

Variable	Maximum for Barrel	Maximum for Endcap
$p_{T,Trk}/p_T$	0.09	0.04
$E_{T,ECAL}/E_T$	0.07	0.05
$E_{T,HCAL}/E_T$	0.1	0.025
$\sigma_{i\eta i\eta}$	0.01	0.03
$ \phi_{Trk} - \phi_{ECAL} $	0.06	0.03
$ \eta_{Trk} - \eta_{ECAL} $	0.004	0.007
$E_{HCAL}/E_{ECAL}$	0.04	0.025

Table 4: Cuts for electron identification.

Muons are only identified to veto events with muons in the “cleaning” step. The cuts follow the recommendations of [27]. The muons have to be reconstructed in the tracker and the muon chambers and fulfill several additional criteria.

- The global track fit must include at least one muon chamber hit and the  $\chi^2/N_{Dof}$  value must be smaller than 10.
- There must be more than one muon chamber matched.
- The transverse impact parameter must be smaller than  $2\text{ mm}$ . This reduces muons induced by air showers.
- There must be at least one hit in the pixel tracker and ten hits in the tracker.

Apart from that, the transverse momentum has to exceed  $7\text{ GeV}$  and the pseudorapidity  $\eta$  must be below 2.1.

Jets must have a transverse momentum of more than  $15\text{ GeV}$ , the pseudorapidity must be  $|\eta| < 2.4$ . A jet must have at least two constituents and a charged hadron fraction above zero. The neutral hadron fraction, charged EM fraction and neutral EM fraction must all be below 0.99. The jet’s distance from any electron must be  $\Delta R < 0.05$ .

## 4.2 Event Selection

After skimming, the data is analyzed using a version of the program FINDSUSY [26] that has been adapted to use electrons rather than muons. The program uses a cut-based analysis technique to separate the signal from the background.

**Pileup Rew.** The Monte Carlo events are reweighted to match the pileup distribution of the data, see section 4.3.

**Trigger** The analysis uses two HLT triggers, HLT\_Ele17\_CaloIdL\_CaloIsoVL\_Ele8\_CaloIdL\_CaloIsoVL and HLT\_Ele17\_CaloIdT\_CaloIsoVL\_TrkIdVL\_TrkIsoVL\_Ele8\_CaloIdT\_CaloIsoVL\_TrkIdVL\_TrkIsoVL.

**Object Id** Electrons, muons and jets are identified, see section 4.1.

**Cleaning** This step includes various cuts. There must be at least one vertex. Events with muons are rejected. Apart from that, there are cuts to reduce the noise in the electromagnetic and the hadronic calorimeter. Events are vetoed if the noise of the energy in one electromagnetic calorimeter is greater than  $3\text{ GeV}$  and the ratio of the energy of the hottest cell and the energy in the  $3 \cdot 3$  matrix of cells around it is greater than 0.9.

**Loose Ele** This cut removes all events with less than two electrons. The first electron must have a transverse momentum of at least  $20\text{ GeV}$ , the second needs  $15\text{ GeV}$ .

**Loose Jet** This step is an analogous cut for the jets. Events with less than two jets are removed, both jets must have a transverse momentum of at least  $30\text{ GeV}$ .

**Electron Id** The leading electron must have a transverse momentum of at least  $20\text{ GeV}$ , the second electron at least  $15\text{ GeV}$ . For the default analysis, this cut is redundant as it is the same as in “Loose Ele”. For double and singlefake, one or both electrons are replaced, making this step necessary. The electrons must also have a distance  $\Delta R > 0.4$  from the nearest jet.

**Jet Smear** The resolution of the jet energy in the Monte Carlo simulation is better than in the data, which has to be corrected by smearing the jets before applying a MET cut. See section 4.5

**MET** Events with a missing transverse energy of more than  $50\text{ GeV}$  are rejected. A high MET is an indicator for neutrinos, which are not formed in the signal process. This makes it possible to discriminate between the signal and backgrounds with neutrinos like  $t\bar{t}$  or  $W+\text{Jets}$ .

**$m_{ee}$**  Cut for the invariant mass of the two electrons. The event is rejected if the invariant mass is lower than  $15\text{ GeV}$  because there is no Monte Carlo for lower invariant masses. This cut also removes invariant masses between  $70$  and  $110\text{ GeV}$  to reduce the Drell-Yan background, which has a peak at  $91\text{ GeV}$ , the mass of the Z boson.

$\Delta\phi$  This cut examines the difference in the azimuth angle of the leading electron and the gaugino. Due to the conservation of momentum, they should move in nearly opposite directions, as they are generated in the same vertex. If  $\Delta\phi$  is smaller than  $2\text{ rad}$ , the event is rejected.

**Charge** This cut selects the events where the two electrons have the same charge.

The cutflow diagram for the analysis can be seen in Fig. 6. Most background is removed by the charge cut.

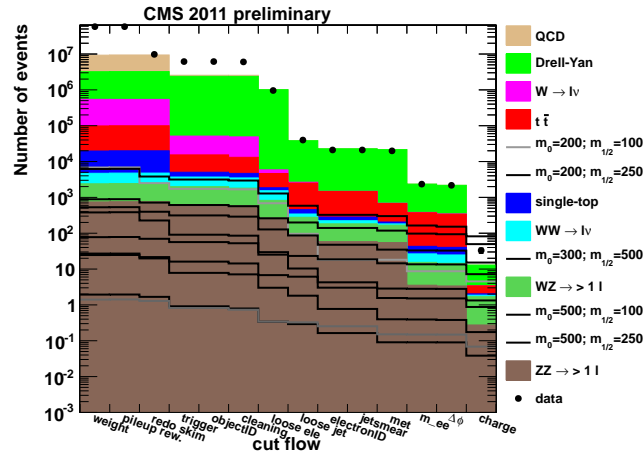


Figure 6: Cutflow diagram for default analysis.

### 4.3 Pileup Reweighting

Due to the high luminosity there are normally several proton-proton interactions per bunch crossing and therefore several primary vertices per event. This phenomenon is called pileup. The pileup distribution (Figure 7) is normally not the same for the data and the Monte Carlo files, so the Monte Carlo files are reweighted to make the distributions match.

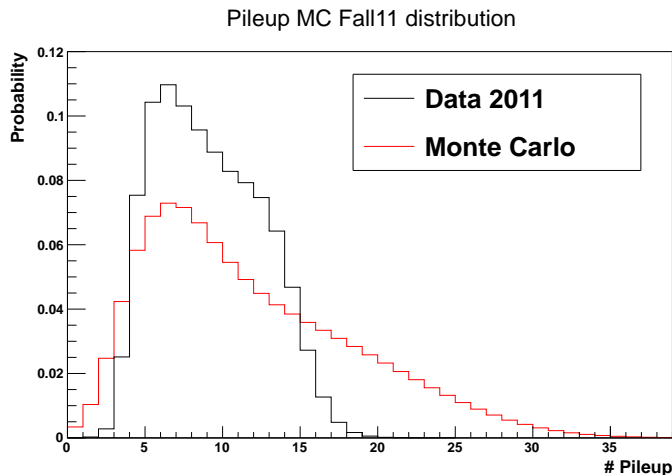


Figure 7: Pileup distributions of data and Monte Carlo files before reweighting.

### 4.4 Tight to Loose Ratio

The tight to loose ratio (T/L) or fakerate method is a data-driven procedure to estimate the QCD and W+Jets background. QCD and W+Jets processes can contribute to the background by creating hadrons that are misidentified as electrons or if electrons within jets are misidentified as isolated electrons and used in the analysis. The data-driven approach is necessary for two reasons. First, these background processes have a very large cross-section making it difficult to generate a sufficient number of Monte Carlo events. Each Monte Carlo event has a contribution equal to a variable number of data events, which is represented by the event weight. Ideally, the weight should be lower than one, so the background can be calculated precisely. For processes with very large cross section, the weight can be much larger than one, up to 9 for the QCD background in this study. If no events from a background process remain, the 95% limit on the expectation value is about three times the event weight, leading to large limits for large event weights. The other problem is the theoretical uncertainty on the QCD predictions .

A better estimate can be made using the tight to loose ratio. A tight electron is an electron that fulfills the criteria of the event selection. The criteria for loose electrons are less rigid, the relative isolation may be up to 0.4 and the first three cuts in table 4 are removed. All tight electrons are also loose electrons. The tight to loose ratio is the

probability for a loose electron to be tight. It is measured as a function of the transverse momentum and the pseudorapidity  $\eta$  by examining data events with exactly one loose electron which may or may not be tight. The exact procedure is discussed below.

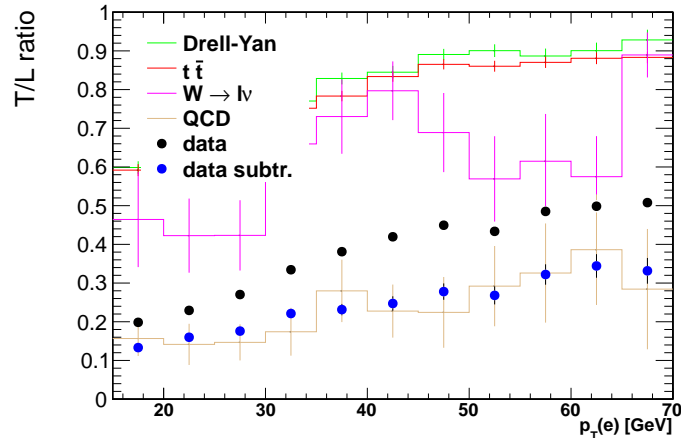


Figure 8: Tight to loose ratio as a function of  $p_T$ . The subtracted ratio is in good agreement with the QCD Monte Carlo.

The analysis is then repeated with either one (single-fake) or both (double-fake) tight electron replaced by a loose electron that is not tight.

Double-fake simulates the QCD background. Each event is weighted with the factor

$$w_{DF} = \frac{T/L^1}{1 - T/L^1} \cdot \frac{T/L^2}{1 - T/L^2} \quad (3)$$

Where  $T/L^1$  and  $T/L^2$  are the tight to loose ratios for the first and the second electron. The sum of all weights is the background estimate.

$$N_{DF} = \sum w_{DF} \quad (4)$$

The single-fake case is used to estimate the background from W+Jet events. Here, the events are weighted with the factor

$$w_{SF} = \frac{T/L^1}{1 - T/L^1} \quad (5)$$

The estimate has to be corrected for the contribution of QCD. The analysis uses events with two loose electrons one of which is tight. It is possible that this tight electron is a misidentified particle from a QCD event. Summing up the weights of all events does

not yield the background from W+Jets events, but the sum of the backgrounds from W+Jets and QCD events. The correct formula for the W+Jets background is:

$$N_{SF} = \sum w_{SF} - N_{DF} \quad (6)$$

The tight to loose ratio has to be measured in a clean QCD environment. This is achieved by subtracting the electroweak background. The tight to loose ratio is measured after the “cleaning” step in the analysis, meaning that the analysis criteria for object Id and trigger matching also apply here. Additionally, the missing transverse energy must be smaller than  $50 \text{ GeV}$ , the total visible hadronic energy (HT) has to be greater than  $50 \text{ GeV}$ . There must be at least one jet with a transverse momentum above  $40 \text{ GeV}$  and, as already mentioned, exactly one loose electron. Electrons are rejected if their transverse momentum is smaller than  $15 \text{ GeV}$ , or if the azimuth angle difference between the electron and the leading jet is smaller than  $1 \text{ rad}$ .

To exclude electrons from the decay of Z bosons, the analysis looks for another electron and computes the invariant mass. The other electron does not have to meet the requirements for a loose electron. If the invariant mass is between  $71$  and  $111 \text{ GeV}$ , the event is rejected. Electrons from the leptonic decay of W bosons are excluded by a cut for the transverse mass of the electron and the missing energy. The missing transverse energy includes the neutrino produced in the decay. The transverse mass must be below  $40 \text{ GeV}$ .

## 4.5 Jet Smearing

The resolution of the jet energy in the data is worse than in the Monte Carlo samples. This leads to a disagreement as the better resolution lowers the average missing transverse energy. This is corrected for by smearing the jets in the Monte Carlo to reduce the effective resolution.

In the first step, the reconstructed particle flow jets are matched to the generated jets. For each reconstructed jet, the energy of the generated jets within a cone of  $\Delta R = \sqrt{\Delta\eta^2 + \Delta\phi^2} < 0.5$  is summed up to calculate the energy difference  $\delta E$ . The missing transverse energy is then calculated using the formula

$$MET_{smear} = MET_{old} - k \cdot \mathbf{p} \cdot \frac{\delta E}{E} \quad (7)$$

Where  $E$  and  $p$  are the energy and transverse momentum of the reconstructed jet and  $k$  is a parameter with the value  $0.25$ .  $k$  was varied to find the value with the optimal agreement between Monte Carlo and data.

Only reconstructed jets with a transverse momentum greater than  $15 \text{ GeV}$  are smeared. If no match is found for a reconstructed jet,  $\delta E$  is chosen randomly using a Breit-Wigner distribution with a mean value of  $1.77 \text{ GeV}$  and a  $\Gamma$  value of  $16.52 \text{ GeV}$ . These values were obtained by fitting a Breit-Wigner distribution to the observed distribution of  $\delta E$  of the reconstructed jets that could be matched to generated jets, see Fig. 10.

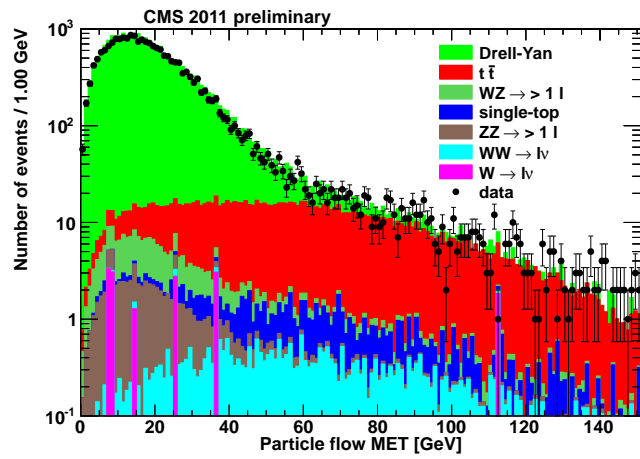
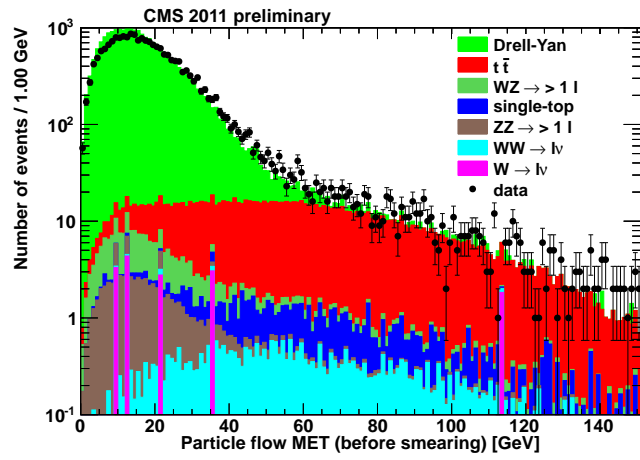


Figure 9: Particle flow MET before (top) and after (bottom) smearing. The agreement between Monte Carlo and data becomes better.

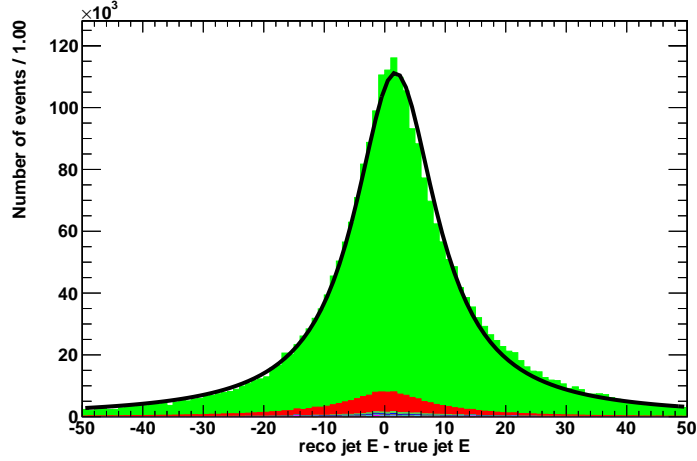


Figure 10: Difference between reconstructed and true jet energy. The Breit-Wigner function fitted to the distribution is used to randomly choose  $\delta E$  for jets that could not be matched.

Figure 9 shows the missing transverse energy distribution before and after smearing. Before smearing, the distribution has an excess in the region below  $20 \text{ GeV}$ , and a deficit at higher energies. Smearing visibly improved the agreement.

#### 4.6 Results

$N_{Data} = 33$  events are selected in data and  $N_{EW} = 12.908 \pm 2.734$  from electroweak backgrounds. The tight to loose ratio method yields an estimate of  $N_{QCD} = 2.016$  and  $N_{W+Jets} = 2.568$  for the QCD and W+Jets backgrounds, the systematic error is assumed to be 30%. The total background is  $N_{Back} = 17.492 \pm 2.904$ , where the error is the Monte Carlo statistics uncertainty. The mass distributions for selectrons and gauginos can be seen in Fig. 11.  $N_{Data}$  is significantly higher than  $N_{Back}$ . This may be due to systematic errors that are not considered in the analysis. The tight to loose ratio method has a high uncertainty. Apart from that, charge misidentification may not be described accurately by the Monte Carlo data. There may also be scale factors due to trigger modeling differences between the data and the Monte Carlo. Another possible source uncertainty is a difference in the lepton Id criteria.

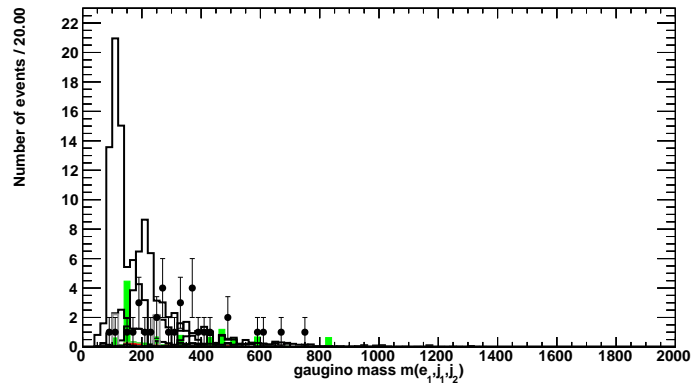
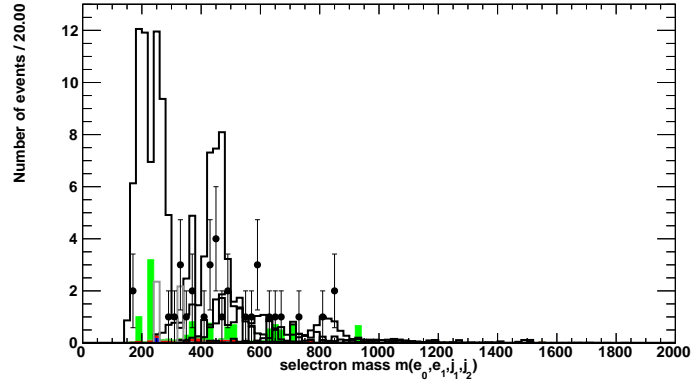


Figure 11: Selectron (top) and gaugino (bottom) mass distribution. The black curves correspond to the signal at the different points in the parameter space.

## 4.7 Calculation of Limits

The results show no evidence for resonant selectron production. Thus, limits for  $\lambda'_{111}$  can be determined, see Table 5. The limits are calculated using a wrapper program developed in the Bachelor thesis of Dominique Dresen [12]. This program uses two packages, ROOSTATS [28] and HIGGS COMBINE [29], making it possible to compare the results. All limits are given at 95% CL.

$M_0 [GeV]$	<b>200</b>	200	300	<b>500</b>	<b>500</b>	600	<b>1000</b>	1000	1600	1600
$M_{1/2} [GeV]$	<b>100</b>	250	500	<b>100</b>	<b>250</b>	850	<b>200</b>	500	450	850
$(0\nu\beta\beta)$	5.5	29.0	134.4	16.7	45.7	470.9	88.8	234.5	368.4	780.9
HIGGS COMBINE	259.2	6.5	8.2	66.5	146.8	21.4	132.8	48.9	284.1	209.3
ROOSTATS (expected)	197.6	4.4	5.6	48.0	102.2	13.9	91.3	34.1	195.8	146.5
ROOSTATS	311.9	6.7	8.2	74.1	149.1	21.2	139.9	50.0	290.9	214.8

Table 5: Limits on  $\lambda'_{111} \cdot 10^3$  calculated using HIGGS COMBINE and ROOSTATS in comparison to the limits from Table 1. The points for which the limit from neutrinoless double beta decay is stricter are in bold print.

For six of the ten points the limits from neutrinoless double beta decay could be improved. The remaining points,  $(M_0 = 200 GeV; M_{1/2} = 100 GeV)$ ,  $(M_0 = 500 GeV; M_{1/2} = 100 GeV)$ ,  $(M_0 = 500 GeV; M_{1/2} = 250 GeV)$  and  $(M_0 = 1000 GeV; M_{1/2} = 200 GeV)$  lie at the lower margin of the parameter space, i.e. they have low values for  $M_{1/2}$ . As the number of observed events is greater than the Monte Carlo expectation, the observed limits are less stringent than the expected limits. There are some differences between the results from ROOSTATS and HIGGS COMBINE, particularly at the point  $(M_0 = 200 GeV; M_{1/2} = 100 GeV)$ . These are due to numerical differences in the calculation of the limits.

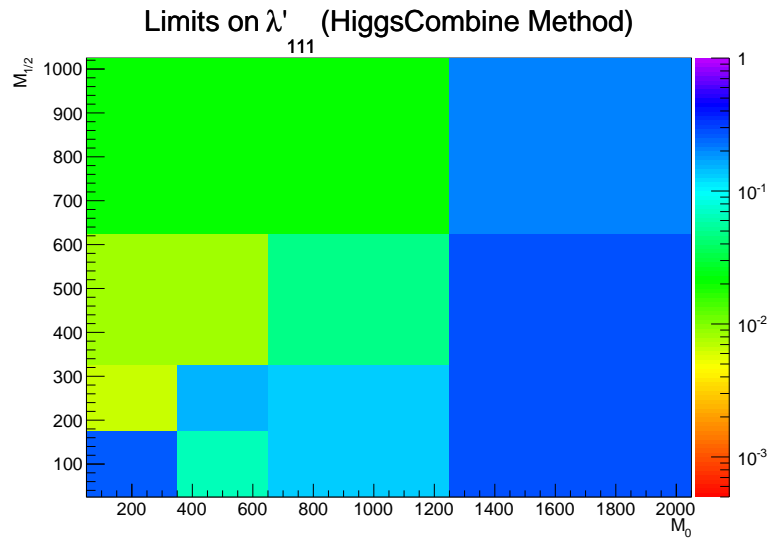


Figure 12: Limits calculated with HIGGSCombine.

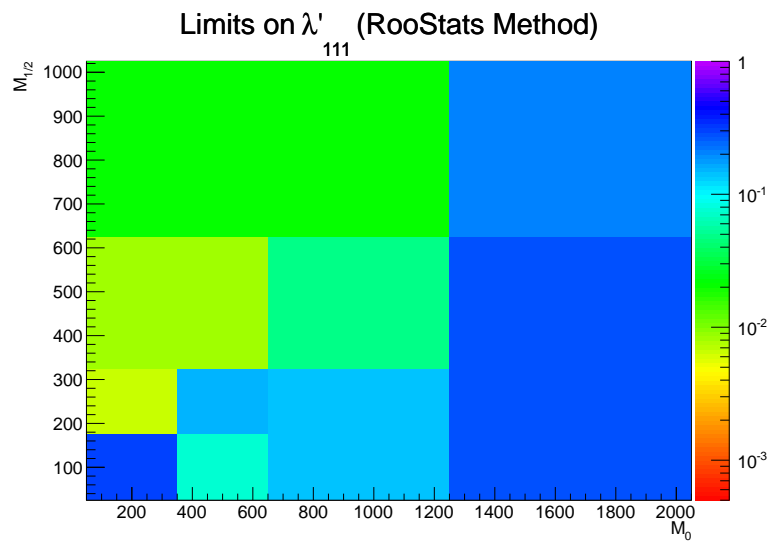


Figure 13: Limits calculated with ROOSTATS.

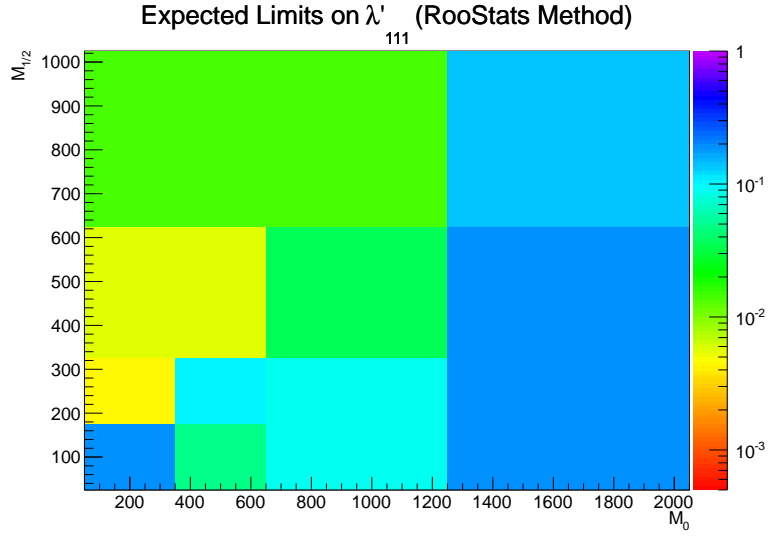


Figure 14: Expected limits calculated with RooStats.

## 5 Conclusion

It was shown that the study is feasible and first results from 2011 data were calculated. The study found no evidence for resonant slepton production at the LHC. For all except four of the ten points in  $M_0, M_{1/2}$  space the limits on  $\lambda'_{111}$  are stricter than previous ones from neutrinoless double beta decay, meaning that this method can improve the results.

## Acknowledgements

I would like to thank Prof. Dr. Thomas Hebbeker for the opportunity to write this thesis. My special thanks go to my supervisor Dr. Martin Weber for always having time for me, his invaluable support and advice and for proofreading this thesis.

I would also like to thank the RPV-Susy group at Physics Institute IIIA for the great working atmosphere.

In particular, I would like to thank Matthias Endres for helping me with the tight to loose ratio method and technical difficulties, and Dominique Dresen for helping me with the limit calculation.

## References

- [1] S.P. Martin: A Supersymmetry Primer, hep-ph/9709356v6.
- [2] A. Salam: Weak and electromagnetic interactions, in Elementary Particle Theory – Relativistic Groups and Analyticity, pages 367–377, John Wiley & Sons, 1968.
- [3] S. Weinberg: Phys. Rev. Lett. 19 (1967) 1264.
- [4] M. Gell-Mann, Y. Ne’eman: Frontiers in Physics, New York, 1964.
- [5] D. Carmi, A. Falkowski, E. Kuflik, Tomer Volansky, Jure Zupan: Higgs After the Discovery: A Status Report, arXiv:1207.1718v3
- [6] L. Ibáñez, G. Ross: Nuclear Physics B 368 (1992) 3—37
- [7] B.C. Allanach, A. Dedes, H.K. Dreiner: The R-Parity Violating Minimal Supergravity Model, arXiv:hep-ph/0309196v5.
- [8] B.C. Allanach, A. Dedes, H.K. Dreiner: Bounds on R-parity Violating Couplings at the Weak Scale and at the GUT Scale.
- [9] H.K. Dreiner, M. Hanussek, S. Grab: Bounds on R-parity violating couplings at the grand unification scale from neutrino masses.
- [10] B.C. Allanach: Comput. Phys. Commun. 143 (2002) 305-331, hep-ph/0104145.
- [11] B.C. Allanach and M.A. Bernhardt: Comput. Phys. Commun. 181 (2010) 232, arXiv:0903.1805.
- [12] D. Dresen: Suche nach resonanter Smyon-Produktion mit dem CMS Experiment, Bachelor thesis, RWTH Aachen, 2012
- [13] B. C. Allanach, C.H. Kom, H. Päs: LHC and B physics probes of neutrinoless double beta decay in supersymmetry without R-parity, arXiv:0903.0347v3.
- [14] M. Hirsch, H.V. Klapdor-Kleingrothaus, S.G. Kovalenko: New Constraints on R-Parity-Broken Supersymmetry from Neutrinoless Double Beta Decay.
- [15] A.S. Barabash: Double Beta Decay: Historical Review of 75 Years of Research, arXiv:1104.2714v2 [nucl-ex]
- [16] H.V. Klapdor-Kleingrothaus et. al.: Latest Results from the Heidelberg-Moscow Double-Beta-Decay Experiment, arXiv:hep-ph/0103062v1.
- [17] M. Bongrand: Results of the NEMO-3 Double Beta Decay Experiment, arXiv:1105.2435v1 [hep-ex].
- [18] R. Barbier, C. Bérat<sup>2</sup>, M. Besançon, M. Chemtob, A. Deandrea, E. Dudas, P. Fayet, S. Lavignac, G. Moreau, E. Perez and Y. Sirois: R-Parity-violating Supersymmetry.

- [19] C. Autermann: Resonant Second Generation Slepton Production at the Tevatron, 2006, Ph. D. thesis
- [20] CMS Physics Technical Design Report Volume I: Detector Performance and Software.
- [21] P. Buning et al.: LHC design report, CERN 2004-003-v2.
- [22] <http://cms.web.cern.ch>
- [23] <http://web.physik.rwth-aachen.de/~hebbeker/cms-muon-system-aachen/index.html>
- [24] <https://twiki.cern.ch/twiki/bin/view/CMS/SimpleCutBasedEleID>
- [25] <https://twiki.cern.ch/twiki/bin/viewauth/CMS/ACSusyAnalysis>
- [26] <https://twiki.cern.ch/twiki/bin/viewauth/CMS/Aachen3ARPV>
- [27] <https://twiki.cern.ch/twiki/bin/view/CMSPublic/SWGuideMuonId>
- [28] <https://twiki.cern.ch/twiki/bin/view/RooStats/WebHome>
- [29] <https://twiki.cern.ch/twiki/bin/viewauth/CMS/HiggsCombinationInstructions>
- [30] N. Kidonakis: Next-to-next-to-leading-order collinear and soft gluon corrections for t-channel single top quark production, arXiv:1103.2792.v1
- [31] N. Kidonakis: Higher-order corrections to top-antitop pair and single top quark production, arXiv:0909.0037.v1
- [32] M. Endres: Search for Resonant Slepton Production in a DiMuon + Jets Final State with CMS Data, Master thesis, RWTH Aachen, to be published
- [33] L. Sonnenschein, III. Physikalisches Institut A, RWTH Aachen: private communication